Peeling of graphene/molybdenum disulfide heterostructure at different angles: A continuum model with accommodations for van der Waals interaction

ZiXiong Wei [a,b], Kui Lin [a,b], XiaoHe Wang [a,b], Ya-Pu Zhao [a,b,*]

[a] *State Key Laboratory of Nonlinear Mechanics, Institute of Mechanics, Chinese Academy of Sciences, Beijing 100190, China*
[b] *School of Engineering Science, University of Chinese Academy of Sciences, Beijing 100049, China*

A B S T R A C T

Being the key process of a promising scalable production method, mechanical peeling is often used to construct high-quality van der Waals (vdW) heterostructures. By combining molecular dynamics (MD) studies and theoretical analysis, the investigation of the process of peeling heterostructures at different angles is reported. Taking vdW interaction into account, we present a theory that considers the effects of peeling angles on peeling forces. The theory is verified with results of MD simulations and found to describe the stable peeling stage well. Furthermore, there is a characteristic length at the initial stage of peeling, which reflects the bending and interfacial properties of the layered materials during peeling and indicates the influence of peeling angles on transition from unstable peeling to stable peeling. Our findings could help to understand the peeling mechanisms of 2D material interfaces and may give a guidance for the construction of better-quality and more complex vdW heterostructures.

1. Introduction

The monolayer graphene was successfully peeled from highly oriented pyrolytic graphite [1] in 2004, and peeled-off two-dimensional (2D) materials was shown to exist stably at room temperature and in air [2,3]. Since then, the family of 2D materials has attracted significant interest due to their outstanding structural, mechanical [4], electrical [5,6], and optical [7] properties, which are dramatically different from those of their three-dimensional counterparts [8]. As the derivatives of 2D materials, van der Waals (vdW) heterostructures have emerged. The in-plane atoms in each 2D monolayer are chemically bonded, and adjacent layers are weakly bonded by the vdW interaction. There is no chemical bonding between different layers, making it possible to create various heterostructures by separating, mixing, and matching atomic layers with different properties. The unique structure equips the vdW heterostructures with novel electronic and optoelectronic properties [9], which renders a variety of applications, such as vertical transistors, plasmonic devices [8], light-harvesting devices [9], etc.

Various applications require the mass productions of heterostructures. To this end, a scalable approach to assemble the vdW heterostructures is desired. To build heterostructures, the basic principle is to stack different layers of the 2D materials on top of each other [10] (Fig. 1a, b), which is called direct mechanical assembly [8] or exfoliation and restacking approach [9]. This method is able to create more complex heterostructures with atomically clean interfaces. The process can be divided into three steps: Preparing the 2D materials, transferring the 2D materials to the substrates, using micromanipulators until the two materials contact to form the heterostructures. During the assembly process, sacrificial polymer membranes are used to transfer 2D materials. In the end of the transfer process, they are directly dissolved to obtain heterostructures [11]. Unfortunately, the residue from the process would be left on the heterostructures and hinder further operations [8,9]. The residues not only increase the surface roughness and cause bubbles or blisters but also give rise to chemical doping [12]. Moreover, experimental operations require much time and lack reproducibility [13], thus making the scalable production arduous. Furthermore, significant efforts of the bottom-up methods, such as the direct growth [14,15] and chemical vapor deposition [16,17], have been utilized to grow vertical heterostructures. The bottom-up strategy is likely to be the technique for scalable production of the vdW heterostructures [8]. However, for growing 2D materials on top of substrates, the weak vdW interaction will not form the continuous monolayers growth but results
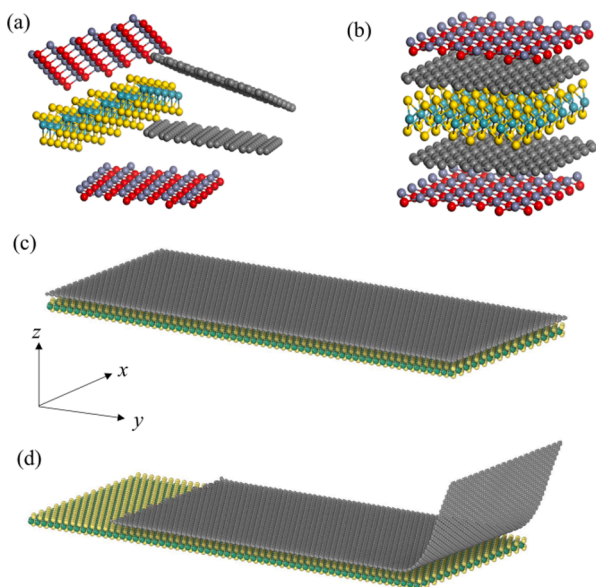

Fig. 1. The vdW heterostructures. (a) Mechanical assembly stacking. (b) Multilayer vdW heterostructure. (c) Atomic model of graphene/MoS$_2$ heterostructure (upper: graphene, lower: MoS$_2$). (d) Atomic illustration of peeling process.

in island growth [10]. In addition, the growing process is affected by the highly sensitive growing conditions of 2D materials [9].

For the transfer process of the mechanical assembly method, it is possible to achieve cleaner multilayer stacking if the polymer membranes are peeled off instead, making this approach a better way to construct better-quality vdW heterostructures. Therefore, mechanical peeling is critical for the assembly process, and peeling force plays an important role during the peeling process. Earlier studies on mechanical peeling behavior at nanoscale focus on carbon nanotubes [18,19] and nanoribbon [20]. For mechanical peeling of 2D materials, most studies focused on peeling from rigid substrate at certain angles [20–23]. Zhang et al. [22] compared the peeling of graphene and hexagonal boron-nitride from copper or silicon substrate at 45° in both dry and water environments. Tang et al. [23] experimentally peeled monolayer to multilayer MoS$_2$ from MoS$_2$ crystal at an inclined angle and found abrupt force drops which correspond to the formation of kinks during the peeling process. Chen et al. [21] simulated the peeling process of graphene sheet from copper substrate with a corrugated surface at 45°, 90° and found the peeling force is sensitive to the peeling angle. The work by Lin and Zhao [24] focused on the situation of peeling at 90° and how to explain the peak peeling force in the initial stage of peeling. However, the detailed effects of peeling angles on peeling behavior of 2D materials are unclear. Moreover, the mechanics analysis of peeling one 2D material can be applied to another one as long as the relevant parameters (i.e., interfacial energy, elastic modulus and so on) are used, which is flexible and convenient to analyze the peeling process of different 2D materials. Thus, a deeper understanding of peeling angle and force is critical for the mechanical peeling process, which provides a guidance in the assembly of the vdW heterostructures.

In this work, the mechanical peeling process of the graphene/molybdenum disulfide (MoS$_2$) heterostructure is investigated to understand the peeling behavior. Firstly, the peeling processes at different angles ranging from 0° to 90° are simulated by using molecular dynamics (MD) method. The peeling force is obtained by calculating the gradient of graphene potential energy along the peeling direction. Then, a peeling theory accounting for the vdW interaction and peeling angle is presented. The validity of our theory is verified with the results of simulations. Finally, we find a characteristic length that is a crucial parameter revealing the transitions from unstable peeling to stable

peeling. Our study aims to clarify the peeling mechanisms of the vdW heterostructures at different angles and provide an insight into the better construction of scalable heterostructures.

2. Model and methodology of MD simulations

To understand the detailed behavior of peeling process, a set of atomic simulations of peeling graphene/MoS$_2$ heterostructure are carried out by the MD method. For graphene/MoS$_2$ heterostructure, due to the "self-cleansing" mechanism [8], the MoS$_2$ substrate can be atomically flat, thus making the analysis for the peeling process relatively easy without considering the substrate surface roughness. The atomic computational model is with a suspended graphene sheet adhered to a MoS$_2$ substrate (Fig. 1c). The upper rectangular-shaped graphene sheet consists of 6400 carbon atoms with the dimensions of 192 Å × 82 Å for the length and width. It is peeled from the same size lower MoS$_2$ layer (Fig. 1d), which is comprised of 1800 Mo atoms and 3600 S atoms. The initial distance between C atoms and top layer S atoms is 3.5 Å.

The adaptive intermolecular reactive empirical bond order (AIREBO) potential [25] derived from the second-generation Brenner potential [26] is adopted to model the interactions of C-C atoms in graphene, which has widely been adopted to study the thermal and mechanical properties of graphene [27,28]. The Stillinger-Weber potential with a developed parameterization set for the MoS$_2$ monolayer is used to describe the atomic interactions within the MoS$_2$ [29] layer, which has been proved to be able to well reproduce the thermal and mechanical properties of MoS$_2$. The 6–12 Lennard-Jones (LJ) potential is adopted to describe the vdW interaction between graphene and MoS$_2$, which is given by [30–32]:

$$V(r) = 4\varepsilon \left[\left(\frac{\sigma}{r} \right)^{12} - \left(\frac{\sigma}{r} \right)^{6} \right] \tag{1}$$

where r is the distance of the interacting atoms, ε is the depth of the potential (i.e., the bond energy at the equilibrium), σ is a parameter determined by the equilibrium distance when interacting potential equals to zero. The energy and distance parameters in the LJ potential are $\varepsilon = 3.95$ meV and $\sigma = 3.625$ Å [33], which are the equivalent potential parameters for the interaction between single-layer of MoS$_2$ and single-layer of graphene. These potential parameters were determined by fitting to the interlayer spacing and the binding energy from density-functional theory results [24,34]. The cutoff distance of LJ potential is 12 Å.

Periodic boundary conditions are applied along the in-plane x-direction to remove the edge effect, with the free boundary condition along the y- and z-directions to allow the graphene to move freely. The MoS$_2$ substrate layer is fixed along y- and z-directions. Prior to peeling, the heterostructure system is relaxed 5000 time steps. The canonical ensemble NVT (constant number of atoms, volume and temperature [35]) is employed in the MD simulations while the temperature is regulated at a constant 0.1 K by Nosé [36]-Hoover [37] heat bath method. The lower temperature of 0.1 K compared to regular 300 K is meant to prevent large thermal vibrations. The time step is 1 fs. The conjugate-gradient algorithm is employed to minimize the energy, with the tolerance of 10^{-7} for energy and force. The energy minimization during the peeling is to make the configuration of the system in an equilibrium state. To simulate the peeling processes at different angles, the first column of atoms at one end of graphene sheet is set to move along the zigzag direction, with different displacements along y- and z-directions at each time step while keeping the velocity the same value. Then, 5 ps simulations are performed for the relaxation of the structure.

All MD simulations in this work are performed using the publicly available simulation code package large-scale atomic/molecular massively parallel simulator (LAMMPS) [38], with the OVITO (Open Visualization Tool) package used for visualization [39].

3. Results and discussion

3.1. Simulation results

As shown in Fig. 2, a set of simulations are conducted at different peeling angles, ranging from 0° to 90°. During the peeling process, the peeled-off graphene part displays oscillation which looks like a wave (Fig. 3) and the oscillation is more obvious for peeling angles less than 45°. This is because once detached from the substrate, the peeled-off part is free from the vdW interaction and will go through a relaxation process resulting in the wave-like oscillation. The non-flat relaxation configurations have resemblance with the structures of graphene observed by transmission electron microscopy [40,41].

The potential energy of graphene can be easily acquired from MD simulations. Since we neglect the thermal fluctuations, the static peeling force is what we consider. By calculating the gradient of graphene's potential energy along the peeling direction, the peeling forces at different peeling angles are obtained. The directional gradient of potential energy is acquired through the calculation of the first derivative of outputted potential energy from simulation result with respect to the displacement at each different angle. As shown in Fig. 4, there is a sudden increase of the force in the initial peeling process. This is due to the significant fluctuation of the kinetic energy of the heterostructure system when the atoms of the peeling front go through the transition from static status to dynamic status. Then, the peeling forces decrease, and the degree of decline becomes more drastic with increasing peeling angles. Besides, with the increase of peeling angles, initial maximum peeling forces decrease. In addition, after the initial peeling stage, the peeling forces fluctuate. The fluctuation is relatively sharp for the peeling length less than 75 Å and is more obvious at small peeling angles. It is in consistent with the oscillatory behaviors of the peeling part as discussed above (Fig. 3).

The fluctuation can be explained by the "accumulation-peeling mechanism" [42]. The peeling force is applied on the graphene sheet. Before the peeling process actually begins, the force will propagate along the graphene sheet. Then, the stress resulting from the peeling force gradually increases until the perpendicular component reaches the maximum value of the vdW force between the heterostructure. Finally, the peeling process continues until the sheet is completely peeled off from the substrate. As soon as the force is strong enough to peel the graphene, the contact part of graphene is peeled causing the fluctuation of the curve. The sudden change in force is because after the peeling process is finished and peeling stops, the stress begins to decrease immediately making itself less than the adhesion force. In addition, the
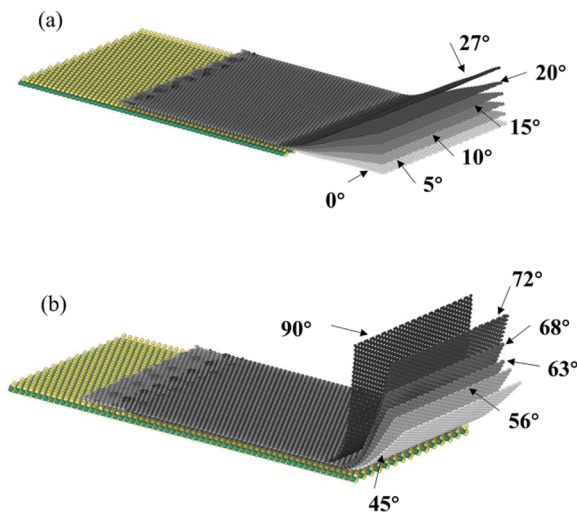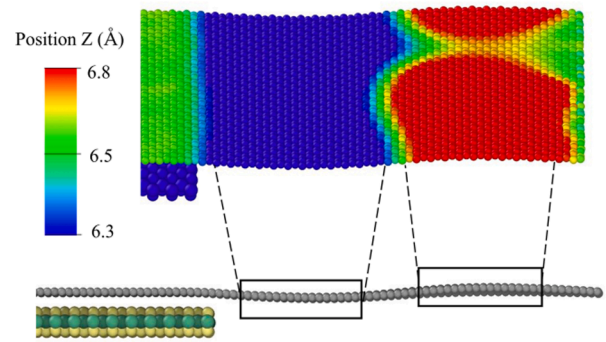

Fig. 3. The relaxation configuration of peeled-off part of the graphene sheet during the peeling process.

adhesion energy between the heterostructure is reduced suddenly because the adhered part is peeled.

After the sharp fluctuations, as can be seen in Fig. 4, the peeling force is a relatively constant value in steady stage. This character is in consistent with the observations of Refs [24,43]. For further analysis, special attention should be emphasized on the constant peeling forces at different angles, which are obtained by calculating the average values of forces in steady peeling stage.

3.2. Theoretical analysis of peeling process accounting for the vdW interaction

For the two-layer graphene/MoS$_2$ heterostructure, to peel the graphene sheet off from the MoS$_2$ substrate, the work done by the peeling force should exceed the adhesion energy between the layers. The expression of adhesion energy needs a further analysis.

As shown in Fig. 5, the following coordinate system is established based on the atomic structure of heterostructure. The graphene layer is parallel to the MoS$_2$ layer, and h denotes the distance between two layers. The thicknesses of graphene and MoS$_2$ are t and T, respectively. To establish a generalized expression, carbon atoms on the graphene is homogenized and represented by volume density ρ_1 (i.e., the number of atoms per unit volume). Therefore, the number of atoms in an infinitesimal volume dV is $\rho_1 dV$. Similarly, Mo and S atoms on the MoS$_2$ layer were represented by volume density ρ_2. The number of atoms over an infinitesimal volume dV is $\rho_2 dV$.

Based on Eq. (A.3), the adhesion energy per unit area (the detailed expression can be seen in the Appendix A) is:

$$\Phi = 4\pi\rho_1\rho_2 tT\varepsilon\sigma^6\left(\frac{\sigma^6}{5h^{10}} - \frac{1}{2h^4}\right) = \frac{HtT}{\pi}\left(\frac{\sigma^6}{5h^{10}} - \frac{1}{2h^4}\right) \quad (2)$$

where $H = 4\pi^2\varepsilon\rho_1\rho_2\sigma^6$, which is the Hamaker constant. At the mesoscopic scale, the Hamaker constant accounts for the strength of the interaction and the density of the surfaces [44] on the order [35] of 10^{-19} J.

From Eq. (A.2), if the thicknesses of upper and lower layer are infinite, the adhesion energy per unit area can be written as:

$$\Phi = \frac{\pi}{3}\rho_1\rho_2\varepsilon\sigma^6\left(\frac{\sigma^6}{30h^8} - \frac{1}{h^2}\right) = \frac{H}{12\pi}\left(\frac{\sigma^6}{30h^8} - \frac{1}{h^2}\right) \quad (3)$$

which is the same result as those of previous work of Jiang et al. [45] and Zhao et al. [46].

The atom number density of graphene [46] is 0.3818 Å^{-2}. Then, using the thickness of graphene $t = 3.35$Å, the volume density is calculated as 0.1138 Å^{-3}. In addition, the atom number density of MoS$_2$ was calculated to be $\rho_2 = 0.2269$ Å^{-3}. The adhesion energy as the function of the distance magnitude between two layers of graphene/ MoS$_2$ heterostructure is shown in Fig. 6. The thickness of MoS$_2$ layer is negligible compared with those of the length and width, thus, Eq. (2) is

Fig. 2. MD simulations of peeling at different angles. (a) 0°, 5°, 10°, 15°, 20°, 27°. (b) 45°, 56°, 63°, 68°, 72°, 90°.
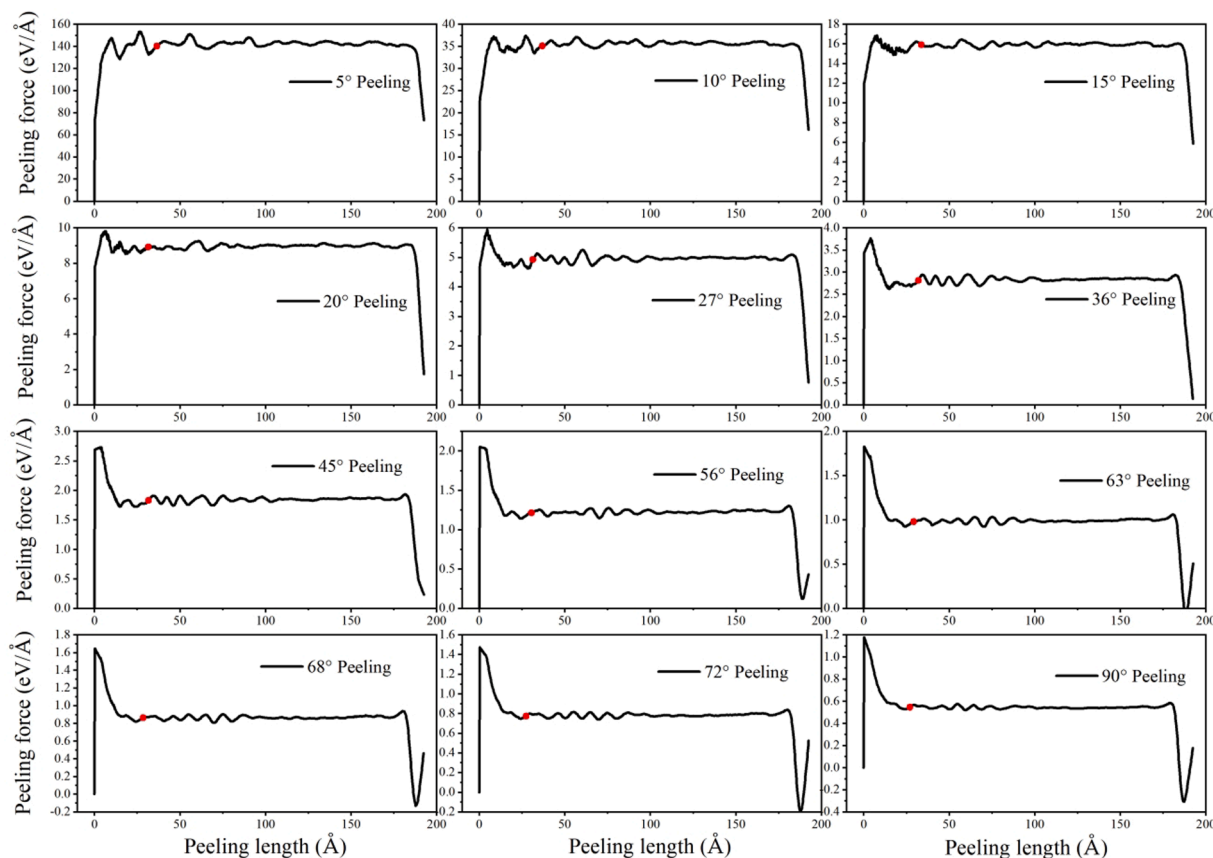
Fig. 4. Comparison of peeling forces for the graphene sheet at different angles. The red points are the reference points indicating the transition from initial peeling to stable peeling.
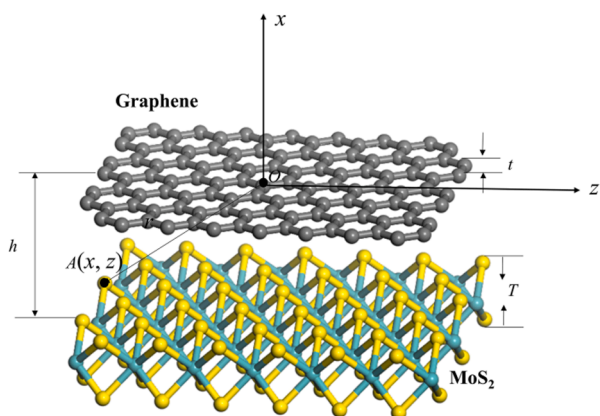

Fig. 5. The coordinate system and an atomic schematic diagram of graphene/MoS$_2$ heterostructure.

Fig. 6. Adhesion energy between graphene/MoS$_2$ heterostructure.

taken for further analysis.

Considering the mechanical peeling process of graphene sheet from flat and adhesive MoS$_2$ substrate as shown in Fig. 7, where a peeling force F is applied on the right end of the graphene sheet with a peeling angle θ, we focus on establishing an analytical expression for the relation between the peeling angle θ and the peeling force F. In the peeling process, the quasi-static and plane strain conditions are assumed. The thermal effect is neglected in order to prevent the kinetic peeling force from the thermal fluctuations. The upper graphene sheet is taken as the 1D Euler-Bernoulli beam [47,48]. The Euler-Bernoulli beam theory assumes the linear elastic material behavior and neglects the shear forces. Moreover, graphene is taken as elastic material for the analysis [49–51].
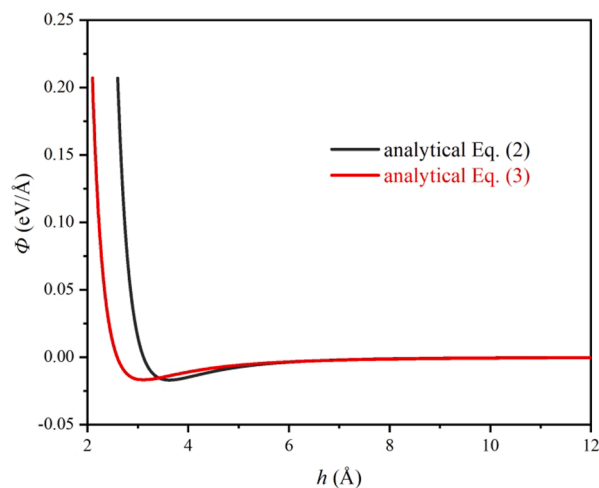
The mechanical behavior of 2D materials can be described by the continuum elasticity theory. The mechanical parameters of graphene used in this study are summarized in Table 1.

In order to peel adhering graphene sheet from adhesive MoS$_2$ substrate, the sufficient peeling force must be provided. During the peeling process, the external work done by the applied peeling force can be converted into the internal elastic energy, the adhesion energy required to separate the heterostructure and the friction energy due to the sliding of graphene sheet. These three kinds of energy can be included as the internal energy.
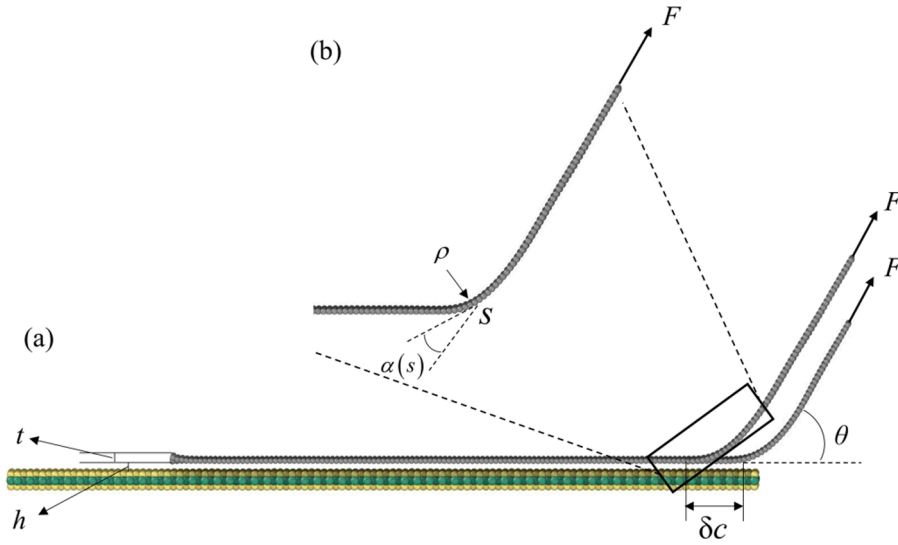
Fig. 7. Schematic of atomic peeling model. (a) Schematic illustration of the mechanical peeling process. (b) 2D sheet peeled off from the substrate.

Table 1
Mechanical parameters used in this work.

Young's modulus [60] E (TPa)	1.23
Bending modulus [48] D (eV)	2.1
Thickness of graphene [61] t (Å)	3.35

The principle of the virtual work is used in this study to derivate the expression of the peeling force. In variational form we have:

$$\delta E_{\text{external}} = \delta E_{\text{internal}} = \delta E_{\text{elastic}} + \delta E_{\text{adhesion}} + \delta E_{\text{friction}} \tag{4}$$

Firstly, by giving an infinitesimal virtual displacement δu of the peeling force along the peeling direction, the virtual external work changes by:

$$\delta E_{\text{external}} = \boldsymbol{F} \cdot \delta \boldsymbol{u} \tag{5}$$

By denoting an infinitesimal virtual length δc as peeled-off length of graphene caused by the δu (Fig. 7a), the virtual displacement can be expressed by δc as:

$$|\delta \boldsymbol{u}| = \delta c(1 - \cos\theta) + \delta c \frac{F}{btE} \tag{6}$$

where E is the Young's modulus of the graphene sheet, b and t are the width and thickness of the graphene sheet, respectively. The first term $\delta c(1 - \cos\theta)$ of the right side of Eq. (6) is the displacement caused by the detachment of the length δc. The second term $\delta cF/btE$ is the additional elastic deformation resulting from the length δc being stressed [52]. The virtual external work done by the applied peeling force can then be calculated by:

$$\delta E_{\text{external}} = \boldsymbol{F} \cdot \delta \boldsymbol{u} = F\delta c(1 - \cos\theta) + \delta c \frac{F^2}{btE} \tag{7}$$

Secondly, for elastic graphene sheet, the internal elastic energy (i.e., strain energy) corresponds to the work done by the internal forces and elastic deformations [47]. The virtual internal force can be characterized by stress tensor σ_0 and elastic deformation can be denoted by the virtual Cauchy strain tensor $\delta\boldsymbol{\varepsilon}_0 = \frac{1}{2}\left(\nabla\delta\boldsymbol{u} + (\nabla\delta\boldsymbol{u})^{\mathrm{T}}\right)$. Thus, the virtual strain energy is:

$$\delta E_{\text{elastic}} = \iiint_{V_{\text{graphene}}} \sigma_0 : \delta\boldsymbol{\varepsilon}_0 dV \tag{8}$$

where σ_0 and $\delta\varepsilon_0$ are the stress and strain tensor of graphene sheet,

respectively. During the peeling process, the internal elastic energy E_{elastic} is composed of the stretching energy E_{stretch} and bending energy E_{bend} that arise from the stretching deformation and bending deformation of the graphene (i.e., $E_{\text{elastic}} = E_{\text{stretch}} + E_{\text{bend}}$), respectively. According to the Euler-Bernoulli beam theory, the shear-lag model is not taken into account and the stretching energy density of the peeling graphene sheet is uniformly distributed, the virtual stretching energy can be expressed as:

$$\delta E_{\text{stretch}} = \frac{1}{2}\sigma_0\delta\varepsilon_0 bt\delta c = \frac{\delta c}{2btE}F^2 \tag{9}$$

The virtual bending energy can be written as:

$$\delta E_{\text{bend}} = \frac{1}{2}D\kappa^2\delta c \tag{10}$$

where D is the bending modulus and κ is the bending curvature. The detailed derivation of bending curvature has been well formulated by Gao et al. [43]. Combining the expression of bending curvature, from Eq. (10), the bending energy can be obtained as [43]:

$$E_{\text{bend}} = \frac{1}{2}\int_0^s Db\kappa^2(s)\mathrm{d}s = \sqrt{2FDb}\left(\sqrt{2} - \frac{\sin\theta}{\sqrt{1 - \cos\theta}}\right) \tag{11}$$

From Eq. (11), it is known for the graphene sheet with given bending modulus and width, the bending energy is dependent on the peeling force and peeling angle. Besides, as indicated by the simulation results, the peeling force at steady peeling stage can be seen as a constant value. As a result, during the steady stage for a fixed peeling angle the bending energy can be regarded as a constant, which means the variation of the bending energy δE_{bend} is equal to zero and can be neglected for our further analysis. The Eq. (8) becomes:

$$\delta E_{\text{elastic}} = \delta E_{\text{stretch}} + \delta E_{\text{bend}} = \frac{\delta c}{2btE}F^2 \tag{12}$$

To obtain the change of the adhesion energy, by using $\gamma = |\Phi|$ to be the absolute value of the adhesion energy per unit area, the expression of the adhesion energy for peeling the length δc is then:

$$\delta E_{\text{adhesion}} = \gamma b\delta c \tag{13}$$

At last, the friction energy $\delta E_{\text{friction}}$ is caused by the sliding of graphene sheet and the intrinsic lattice mismatch of two layered materials [53]. The deformation caused by lattice mismatch can be obtained by using the Cauchy-Born rule as shown in the Appendix C. The friction energy has no effect on the adhesive motion for heterostructures and is

magnitude of at least one order smaller than adhesion energy [54]. Besides, one experimental work by Annett and Cross [55] showed that for sliding of graphene friction is of negligible magnitude compared to interfacial force. Therefore, $\delta E_{\text{friction}}$ is neglected for the analysis. If the corrugation and adhesion energy need to be considered simultaneously, the registry-dependent Kolmogorov and Crespi interlayer potential can be utilized [56].

Therefore, the total variation of the internal energy of the system subjected to the peeling force F is given by:

$$\delta E_{\text{internal}} = \gamma b \delta c + \frac{\delta c}{2btE}F^2 \tag{14}$$

Considering the energy is balanced at the peel-off state, we have $\delta E_{\text{external}} = \delta E_{\text{internal}}$. By using the Hamaker constant $H = 4\pi^2\varepsilon\rho_1\rho_2\sigma^6$, the adhesion energy per unit area is expressed as:

$$\gamma = \frac{HtT}{\pi}\left(\frac{\sigma^6}{5h^{10}} - \frac{1}{2h^4}\right) \tag{15}$$

By combining Eqs. (7), (14) and (15), the peeling equation is obtained as:

$$F^2 + 2F(1 - \cos\theta)btE = \frac{2Eb^2t^2TH}{\pi}\left(\frac{\sigma^6}{5h^{10}} - \frac{1}{2h^4}\right) \tag{16}$$

It should be noted that the Eq. (16) can be reduced to the following form:

$$\left(\frac{F}{b}\right)^2\frac{1}{2tE} + \frac{F}{b}(1 - \cos\theta) = \gamma \tag{17}$$

if we substitute the right side of Eq. (16) with γ. Eq. (17) was given by Kendall [52,57]. Eq. (16) can also be reduced to $\frac{F}{b}(1 - \cos\theta) = \gamma$, if the nonlinear term is neglected [58], which was given by Rivlin [59].

Solving Eq. (16), we have:

$$F = -(1 - \cos\theta)Ebt + \sqrt{[(1 - \cos\theta)Ebt]^2 + \frac{2Eb^2t^2TH}{\pi}\left(\frac{\sigma^6}{5h^{10}} - \frac{1}{2h^4}\right)} \tag{18}$$

which is the formula of relations of peeling force and peeling angle. When the structure is in an equilibrium state, the distance h can be expressed as $h = 2^{1/6}\sigma$, making Eq. (18) become:

$$F = -(1 - \cos\theta)Ebt + \sqrt{[(1 - \cos\theta)Ebt]^2 + \frac{2^{4/3}}{5}\frac{HEb^2t^2T}{\pi\sigma^4}} \tag{19}$$

Combining Eqs. (15) and (18), we have:

$$F = \frac{2b\gamma}{\sqrt{(1 - \cos\theta)^2 + \frac{2\gamma}{Et}} + (1 - \cos\theta)} \tag{20}$$

If we denote F_0 by $F_0 = b\gamma$, then the dimensionless peeling force can be expressed as:

$$\frac{F}{F_0} = \frac{2}{\sqrt{(1 - \cos\theta)^2 + \frac{2\gamma}{Et}} + (1 - \cos\theta)} \tag{21}$$

To verify the validity of the theory developed above, it is compared with the results coming from the MD simulations. The peeling forces at the stable stage for different angles are averaged, after we obtain the peeling force versus peeling length curves. Then, the results are plotted with the theory. As seen in Fig. 8, the theory is matched well with the simulation results. The values of dimensionless forces from theory are larger than the corresponding simulation results. The deviation between simulation results and the curve of theoretical analysis stems from the choices of related parameters in Eq. (21) (i.e., the adhesion energy, the Young's modulus of graphene and the thickness of graphene). Besides, the adhesion energy is also influenced by the thickness of graphene from its mathematical expression. However, for peeling angles less than 10°, the values of forces from simulation results are bigger than the predicted
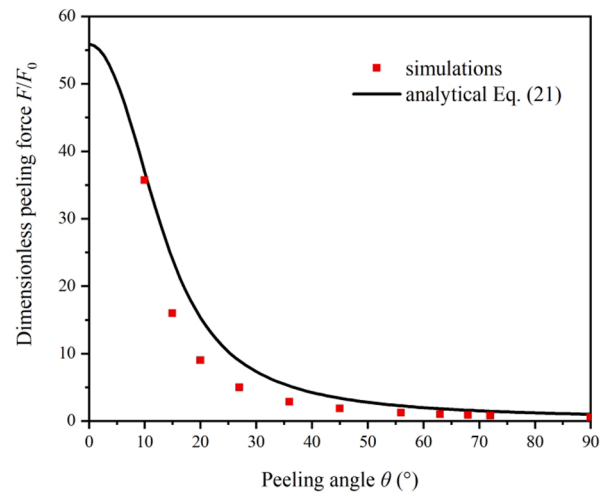

Fig. 8. The evolution of peeling force as the function of varying peeling angles.

values obtained by the theory. This is due to the influence of elastic modulus on the peeling force (Fig. 9). With the decrease of peeling angles, small changes in the value of the elastic modulus will cause relatively large differences of dimensionless peeling force. This effect is obvious for peeling angles less than 30°. Thus, choosing the accurate Young's modulus is crucial.

3.3. Characteristic length at the initial stage of peeling

As can be seen in Fig. 4, after the high peaks of initial peeling force, the curves show decreasing trends and enter a flat plateau. Here, a characteristic length L_M can be identified, which is the length of graphene from initial peeling stage to the steady-state peeling stage. After the peeling force versus peeling length curves are obtained (Fig. 4), the characteristic lengths for different peeling angles are the lengths the reference points (the red points in Fig. 4) refer to. The length varying with changes of peeling angles is shown in Fig. 10. For angles smaller than 90°, the length L_M increases as the peeling angle increases.

To get the expression of the length L_M, we need to understand the unstable peeling stage. Before the peeling direction of graphene sheet is at a certain angle, the front region is firstly flat, then it will gradually rise up to the certain angle. During the process, the deformation the front region goes through can be seen as the bending of a 1D Euler-Bernoulli cantilever beam.

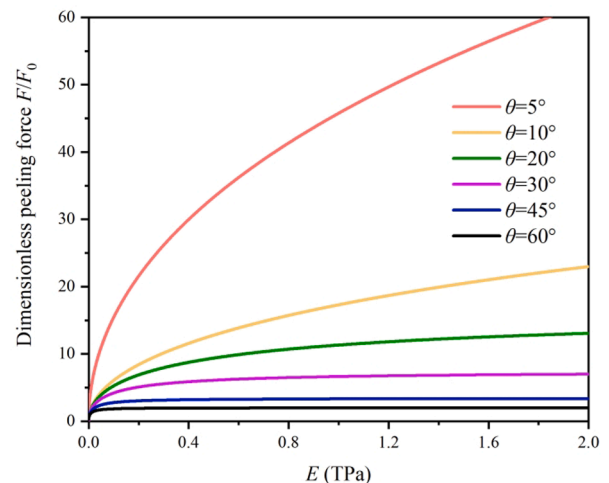By considering the curvature of the bending region:

Fig. 9. Dimensionless peel-off force versus elastic modulus E of graphene.
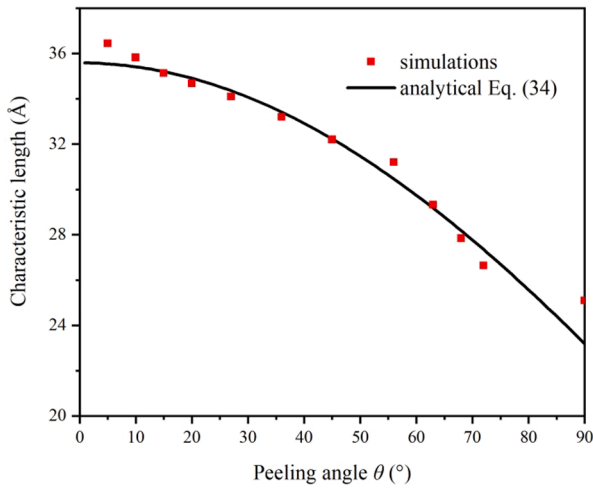
Fig. 10. The characteristic length versus the peeling angles.

$$\kappa(s) = \sqrt{\frac{2F(1 - \cos\alpha)}{Db}} \tag{22}$$

the bending moment can be expressed as:

$$M(s) = Db\kappa(s) = \sqrt{2FDb(1 - \cos\alpha)} \tag{23}$$

For a cantilever beam with length l and bending rigidity EI subjected to a moment M on one end, its deflection w can be expressed as:

$$w = \frac{Mx^2}{2EI} \tag{24}$$

the angle of the corner of the end β is the first order derivative of the deflection, and thus is:

$$\beta = \frac{Ml}{EI} \tag{25}$$

For the graphene sheet, by analogy with the cantilever beam, the characteristic length is $L_M = l$ and bending modulus is $D = EI/b$. Then, substituting Eq. (23) into Eq. (25), we have:

$$L_M = \frac{\beta D}{\sqrt{2FD(1 - \cos\alpha)}} \tag{26}$$

where F is the peeling force, α is the angle between the tangent to the graphene sheet and the direction of the peeling force.

To obtain the characteristic length varying with angle β, we have to get the relation between α and β. According to the geometric relationship, it is easy to obtain the relation $\alpha = \frac{1}{2}\beta$, then we have:

$$L_M = \frac{\beta D}{\sqrt{2FD\left(1 - \cos\frac{\beta}{2}\right)}} \tag{27}$$

However, β is the approximation of $\tan\beta$ for small bending angles. Eq. (27) is only suitable to the situations when bending deformation is small, which is not appropriate for our simulations. Using the derivatives of deflection to the length, for peeling angle θ, we have:

$$\tan\theta = \frac{dw}{dx} \tag{28}$$

For pure bending of beam, we have:

$$\frac{\frac{d^2w}{dx^2}}{\left[1 + \left(\frac{dw}{dx}\right)^2\right]^{3/2}} = \frac{M}{Db} \tag{29}$$

Substituting Eq. (28) into Eq. (29), we have:

$$\frac{d\tan\theta}{\left[1 + (\tan\theta)^2\right]^{3/2}} = \frac{M}{Db} dx \tag{30}$$

Integrating both sides of Eq. (30), we have:

$$\frac{\tan\theta}{\left[1 + (\tan\theta)^2\right]^{1/2}} = \int_0^{L_M} \frac{M}{Db} dx = \frac{ML_M}{Db} \tag{31}$$

Then, we have:

$$L_M = \frac{Db}{M} \frac{\tan\theta}{\left[1 + (\tan\theta)^2\right]^{1/2}} \tag{32}$$

Combining Eq. (23) and $\alpha = \frac{1}{2}\theta$, we can finally get:

$$\begin{aligned} L_M &= \sqrt{\frac{Db}{2F}} \cdot \frac{\tan\theta}{\sqrt{(1 + \tan^2\theta)\left(1 - \cos\frac{\theta}{2}\right)}} = \sqrt{\frac{Db}{2F}} \cdot \frac{\sin\theta}{\sqrt{1 - \cos\frac{\theta}{2}}} \\ &= \sqrt{\frac{Db}{2F}} \cdot \frac{2\sin\frac{\theta}{2}\cos\frac{\theta}{2}}{\sqrt{1 - \cos\frac{\theta}{2}}} = \sqrt{\frac{2Db}{F}} \cdot \frac{\sqrt{1 - \cos^2\frac{\theta}{2}}\cos\frac{\theta}{2}}{\sqrt{1 - \cos\frac{\theta}{2}}} \\ &= \sqrt{\frac{2Db}{F}} \cdot \sqrt{1 + \cos\frac{\theta}{2}}\cos\frac{\theta}{2} \end{aligned} \tag{33}$$

where $D = 2.1$ eV is taken [48]. For the value of peeling force F, the characteristic length is defined as the length of graphene from initial peeling stage to the steady-state peeling stage, thus the peeling force at the stable stage is important. During the bending process, the peeling force is to work against the adhesion between the heterostructure. Thus, we take $F = 0.54$eV/Å, which is the stable peeling force against adhesion from our simulation results. At the stable peeling stage, we have $\gamma = \frac{F}{b}$, Eq. (33) then becomes:

$$L_M = \sqrt{\frac{2D}{\gamma}} \cdot \cos\frac{\theta}{2} \sqrt{1 + \cos\frac{\theta}{2}} \tag{34}$$

By considering two special conditions $\theta = 0°$ and $\theta = 90°$, for $\theta = 0°$, $\cos\frac{\theta}{2} = 1$, the expression of Eq. (34) becomes:

$$L_M = 2\sqrt{\frac{D}{\gamma}} \tag{35}$$

the value is 35.78 Å, which is slightly smaller than the simulation result. Actually, for $\theta = 0°$, the peeling process proceeds against friction force.

For $\theta = 90°$, Eq. (34) becomes:

$$L_M = \sqrt{\frac{D}{(2 - \sqrt{2})\gamma}} \tag{36}$$

the characteristic length is about 23.4 Å. The length is very close to the elasto-peeling length proposed by Lin and Zhao [24].

By substituting Eq. (15) into Eq. (34), the characteristic length can also be expressed with Hamaker constant as:

$$L_M = 2^{1/3}\sigma^2 \sqrt{\frac{5\pi D}{HtT}} \cdot \cos\frac{\theta}{2} \sqrt{1 + \cos\frac{\theta}{2}} \tag{37}$$

The curve from Eq. (34) with the simulation results is shown in Fig. 10.

For $\theta \geqslant 90°$, we perform a simulation of $135°$ peeling and obtain the peeling force versus peeling length curve. It is found that the dimensionless peeling force is 0.69 from simulation result, which is very close to 0.6 from Eq. (21). It means our theory is applicable for the situation when $\theta \geqslant 90°$. However, the characteristic length is about 25 Å, which is not well matched with the result 12 Å from Eq. (34). This is due to the

effect of bending process. The peeling part of graphene sheet is firstly a flat region. Before the peeling was along a certain direction (i.e., at certain peeling angle), it took relatively longer time to go through the transition stage and thus peel longer length. Thus, the expression for the characteristic length is only appliable for peeling angles less than 90°.

This characteristic length is physically significant: D is the bending rigidity of the peeled graphene, σ denotes the equilibrium distance between the vdW heterostructure, H is the Hamaker constant, which accounts for the strength of the interaction and is influenced by the composition of the surfaces. Hence, it is a crucial parameter that reflects the bending and interfacial properties of the layered materials during peeling.

4. Conclusions

The mechanical processes of graphene peeled from MoS$_2$ substrate at different angles are investigated by conducting MD simulations. By calculating the gradient of graphene's potential energy along the peeling direction, the peeling forces at different angles are obtained. At the initial stage, the peeling forces rapidly increase until the maximum values are reached. The peeling forces then begin to decrease and eventually become stabilized. In addition, the fluctuations on the peeling force curves correspond to the oscillatory behaviors of the peeled part of graphene, which can be explained by the "accumulation-peeling mechanism".

Based on a quasi-continuum method, we present a theoretical analysis coupling traditional peeling theory with the vdW interaction to develop a theory revealing the effects of peeling angles on peeling forces. The peeling forces decrease with the increase of peeling angles. We compare our theory with the results of simulations and they are matched well, which means the theory is capable of describing stable peeling at different angles. For peeling angles less than 10°, the peeling force is sensitive to the elastic modulus of the graphene sheet.

Furthermore, a characteristic length at the initial stage of peeling was found and formalized $L_{\mathrm{M}} = \sqrt{2D/\gamma} \cdot \cos(\theta/2)\sqrt{1 + \cos(\theta/2)}$, which is an important parameter that elucidates the transition from unstable peeling to stable peeling. This characteristic length is characterized by the bending modulus of graphene and adhesion energy between the vdW heterostructure, which means the peeling behavior is influenced by the type of the 2D materials and adhesion energy of interfaces. It can also be written with the Hamaker constant as $L_{\mathrm{M}} = 2^{1/3}\sigma^2\sqrt{5\pi D/HtT} \cdot \cos(\theta/2)\sqrt{1 + \cos(\theta/2)}$. Our findings are aimed at understanding the mechanism behind the peeling process and helping to better construct the vdW heterostructures.

CRediT authorship contribution statement

ZiXiong Wei: Conceptualization, Methodology, Software, Formal analysis, Writing - original draft. **Kui Lin:** Conceptualization, Methodology, Validation, Writing – review & editing. **XiaoHe Wang:** Validation, Writing – review & editing. **Ya-Pu Zhao:** Conceptualization, Methodology, Resources, Writing – review & editing, Supervision, Project administration, Funding acquisition.

Declaration of Competing Interest

The authors declare that they have no known competing financial interests or personal relationships that could have appeared to influence the work reported in this paper.

Acknowledgments

Appendix A. . The adhesion energy between graphene/MoS$_2$ heterostructure

The 6–12 LJ potential $V(r) = 4\varepsilon\left[(\sigma/r)^{12} - (\sigma/r)^6\right]$ is adopted to model the vdW interaction between graphene sheet and MoS$_2$ substrate. As shown in Fig. 5, the distance between the point O (0, 0) on the upper graphene and A (x, z) on the lower MoS$_2$ is $r = \sqrt{x^2 + z^2}$. The interaction energy E between one atom on the graphene and the MoS$_2$ substrate is:

$$
\begin{aligned}
E &= \int_{V_{\mathrm{MoS}_2}} V(r)\rho_2 \mathrm{d}V_{\mathrm{MoS}_2} = 2\pi\rho_2 \int_{-(h+T)}^{-h}\int_0^\infty V(r)z\mathrm{d}z\mathrm{d}x \\
&= 8\pi\rho_2\varepsilon \int_{-(h+T)}^{-h}\int_0^\infty \left[\left(\frac{\sigma}{r}\right)^{12} - \left(\frac{\sigma}{r}\right)^6\right]z\mathrm{d}z\mathrm{d}x \\
&= 4\pi\rho_2\varepsilon \int_{-(h+T)}^{-h}\int_0^\infty \left[\frac{\sigma^{12}}{\left(x^2 + z^2\right)^6} - \frac{\sigma^6}{\left(x^2 + z^2\right)^3}\right]\mathrm{d}z^2\mathrm{d}x \\
&= \frac{2\pi}{3}\rho_2\varepsilon\left[\frac{2}{15}\left(\frac{\sigma^{12}}{h^9} - \frac{\sigma^{12}}{(h+T)^9}\right) - \left(\frac{\sigma^6}{h^3} - \frac{\sigma^6}{(h+T)^3}\right)\right]
\end{aligned}
$$

(A.1)

Then, the adhesion energy Φ per unit area is given as:

$$\Phi = \frac{\rho_1 dA \int_h^{h+t} \frac{2\pi}{3}\rho_2 \varepsilon \left[\frac{2}{15}\left(\frac{\sigma^{12}}{h^9} - \frac{\sigma^{12}}{(h+T)^9}\right) - \left(\frac{\sigma^6}{h^3} - \frac{\sigma^6}{(h+T)^3}\right) \right] dh}{dA}$$

$$= \frac{1}{3}\pi\rho_1\rho_2\varepsilon\sigma^6 \left(\begin{array}{c} \frac{\sigma^6}{30}\left[\left(\frac{1}{h^8} - \frac{1}{(h+t)^8}\right) - \left(\frac{1}{(h+T)^8} - \frac{1}{\left(t+(h+T)^8\right)}\right) \right] \\[2mm] - \left[\left(\frac{1}{h^2} - \frac{1}{(h+t)^2}\right) - \left(\frac{1}{(h+T)^2} - \frac{1}{\left[t+(h+T)\right]^2}\right) \right] \end{array} \right)$$

$$= \frac{H}{12\pi} \left(\begin{array}{c} \frac{\sigma^6}{30}\left[\left(\frac{1}{h^8} - \frac{1}{(h+t)^8}\right) - \left(\frac{1}{(h+T)^8} - \frac{1}{\left(t+(h+T)^8\right)}\right) \right] \\[2mm] - \left[\left(\frac{1}{h^2} - \frac{1}{(h+t)^2}\right) - \left(\frac{1}{(h+T)^2} - \frac{1}{\left[t+(h+T)\right]^2}\right) \right] \end{array} \right) \qquad (A.2)$$

For 2D materials, the size of thickness can be neglected compared to that of length and width, thus, adhesion energy Φ per unit area can also be calculated as:

$$\Phi = \frac{\rho_1 t dA \cdot 2\pi\rho_2 T \int_0^\infty V(r)z dz}{dA}$$

$$= 2\pi\rho_1\rho_2 tT \int_0^\infty \left[\frac{\sigma^{12}}{(x^2+z^2)^6} - \frac{\sigma^6}{(x^2+z^2)^3} \right] dz^2$$

$$= 4\pi\rho_1\rho_2 tT\varepsilon\sigma^6 \left(\frac{\sigma^6}{5x^{10}} - \frac{1}{2x^4} \right) \qquad (A.3)$$

$$= \frac{HtT}{\pi}\left(\frac{\sigma^6}{5x^{10}} - \frac{1}{2x^4} \right)$$

where x is the distance between two 2D layers. From the above analysis, the adhesion energy of the vdW heterostructure due to the vdW interaction can be decided.

Appendix B. . The derivation of bending curvature of graphene

As shown in Fig. 7b, curvilinear coordinate system is established, where s is the curvilinear abscissa and $\alpha(s)$ as the angle between the tangent to the graphene sheet and the direction of peeling force. Then, the curvature of graphene has the form: $\kappa(s) = d\alpha/ds$ and the bending moment can be expressed as: $M(s) = Db\kappa(s)$.

Combining the bending moment and the peeling force, we have:

$$Db\kappa(s) = D\frac{d\alpha}{ds} = F\int_0^s \sin\alpha ds \qquad (B.1)$$

Taking the first order derivation [43] of both sides of Eq. (B.1) and using the expression of curvature, we have:

$$\kappa(s)\frac{d\kappa(s)}{d\alpha} = \frac{F\sin\alpha}{Db} \qquad (B.2)$$

Integrating Eq. (B.2) with boundary condition [43], we have:

$$\kappa^2(s) = \frac{2F(1-\cos\alpha)}{Db} \qquad (B.3)$$

Thus, the bending curvature is given by:

$$\kappa(s) = \sqrt{\frac{2F(1-\cos\alpha)}{Db}} \qquad (B.4)$$

Appendix C. . Lattice mismatch strain obtained by Cauchy-Born rule

For homogeneous continuum deformation, the Cauchy-Born rule is very often used to relate changes in lattice vectors to macroscopic deformation of crystals. The position of a material point $\mathbf{X}$ in the reference configuration (the equilibrium configuration of each undeformed single layer) can be mapped to the point $\mathbf{x}$ in the current configuration (the equilibrium configuration of each deformed layer in heterostructure) via $\mathbf{x} = \mathbf{X} + \mathbf{u}(\mathbf{X})$, where $\mathbf{u}(\mathbf{X})$ is the displacement vector.

The transformation of an infinitesimal line segment from the reference configuration to the current configuration is describe by the deformation gradient $\mathbf{F}$, which is defined as $\mathbf{F} = \partial\mathbf{x}/\partial\mathbf{X} = \mathbf{I} + \partial\mathbf{u}/\partial\mathbf{X}$, where $\mathbf{I}$ is the identity tensor of rank two. If the deformation function be denoted as $\varphi(\mathbf{X}, t)$, the deformation gradient $\mathbf{F}$ can also be defined as $\mathbf{F} = \partial\varphi(\mathbf{X})/\partial\mathbf{X} = (\partial x_i/\partial X_A)e_i \otimes e_A$, where e_i and e_A are the bases of the current configuration and

reference configuration, respectively. Using deformation gradient $\mathbf{F}$, the Green strain tensor $\mathbf{E}$ can be written as $\mathbf{E} = \frac{1}{2}\left(\mathbf{F}^{\mathrm{T}}\mathbf{F} - \mathbf{I}\right)$.

The Cauchy-Born rule views the lattice vectors as infinitesimal material vectors that transform according to:

$$\mathbf{a} = \mathbf{F}\mathbf{A} \tag{C.1}$$

where $\mathbf{A}$ denotes an undeformed lattice vector and $\mathbf{a}$ the same vector in the deformed crystal. Similarly, the related atomic distance $\mathbf{r}_{ij}$ in the current configuration can be obtained from the corresponding relative atomic distance $\mathbf{R}_{ij}$ in the reference configuration as:

$$\mathbf{r}_{ij} = \mathbf{F}\mathbf{R}_{ij} = (\mathbf{I} + \mathbf{H})\mathbf{R}_{ij} \tag{C.2}$$

where $\mathbf{H}$ is the displacement gradient tensor.

For lattice mismatch, it will result in a lattice mismatch strain defined as:

$$\varepsilon_{\mathrm{m}} = \left(a_{\mathrm{combine}} - a_{\mathrm{single}}\right)\big/a_{\mathrm{single}} \tag{C.3}$$

where a_{single} and a_{combine} are the lattice constants of the single and combined material, respectively. The Cauchy strain tensor of graphene and MoS_2 can be expressed as:

$$\boldsymbol{\varepsilon}_{\mathrm{C}} = \frac{1}{2}\left(\mathbf{H} + \mathbf{H}^{\mathrm{T}}\right) = \frac{\partial\varphi(\mathbf{X})}{\partial\mathbf{X}} - \mathbf{I} \tag{C.4}$$

The components of the Cauchy strain tensor are:

$$\begin{pmatrix} \varepsilon_{\mathrm{C1}} \\ \varepsilon_{\mathrm{C2}} \end{pmatrix} = \begin{pmatrix} \dfrac{\partial\varphi(\mathrm{X}_1)}{\partial\mathrm{X}_1} - 1 \\ \dfrac{\partial\varphi(\mathrm{X}_2)}{\mathrm{X}_2} - 1 \end{pmatrix} \tag{C.5}$$

References

[1] Novoselov KS, Geim AK, Morozov SV, Jiang D, Zhang Y, Dubonos SV, et al. Electric field effect in atomically thin carbon films. Science 2004;306(5696):666–9.

[2] Novoselov KS, Jiang D, Schedin F, Booth TJ, Khotkevich VV, Morozov SV, et al. Two-dimensional atomic crystals. Proc Natl Acad Sci USA 2005;102(30):10451–3.

[3] Coleman JN, Lotya M, O'Neill A, Bergin SD, King PJ, Khan U, et al. Two-dimensional nanosheets produced by liquid exfoliation of layered materials. Science 2011;331(6017):568–71.

[4] Akinwande D, Brennan CJ, Bunch JS, Egberts P, Felts JR, Gao H, et al. A review on mechanics and mechanical properties of 2D materials—graphene and beyond. Extreme Mech Lett 2017;13:42–77.

[5] Mak KF, Lee C, Hone J, Shan J, Heinz TF. Atomically thin mos₂: A new direct-gap semiconductor. Phys Rev Lett 2010;105(13):136805.

[6] Yoon Y, Ganapathi K, Salahuddin S. How good can monolayer mos₂ transistors be? Nano Lett 2011;11(9):3768–73.

[7] Splendiani A, Sun L, Zhang Y, Li T, Kim J, Chim C-Y, et al. Emerging photoluminescence in monolayer mos₂. Nano Lett 2010;10(4):1271–5.

[8] Novoselov KS, Mishchenko A, Carvalho A, Castro Neto AH. 2D materials and van der Waals heterostructures. Science 2016;353(6298):aac9439.

[9] Liu Y, Weiss NO, Duan X, Cheng H-C, Huang Y, Duan X. Van der Waals heterostructures and devices. Nat Rev Mater 2016;1(9):1–17.

[10] Geim AK, Grigorieva IV. Van der Waals heterostructures. Nature 2013;499(7459):419–25.

[11] Zomer PJ, Dash SP, Tombros N, van Wees BJ. A transfer technique for high mobility graphene devices on commercially available hexagonal boron nitride. Appl Phys Lett 2011;99(23):232104. https://doi.org/10.1063/1.3665405.

[12] Onodera M, Masubuchi S, Moriya R, Machida T. Assembly of van der Waals heterostructures: Exfoliation, searching, and stacking of 2D materials. Jpn J Appl Phys 2020;59(1):010101. https://doi.org/10.7567/1347-4065/ab5ee0.

[13] Fan S, Vu QA, Tran MD, Adhikari S, Lee YH. Transfer assembly for two-dimensional van der Waals heterostructures. 2D Mater 2020;7(2):022005.

[14] Liu Z, Song Li, Zhao S, Huang J, Ma L, Zhang J, et al. Direct growth of graphene/hexagonal boron nitride stacked layers. Nano Lett 2011;11(5):2032–7.

[15] Zhang C, Zhao S, Jin C, Koh AL, Zhou Yu, Xu W, et al. Direct growth of large-area graphene and boron nitride heterostructures by a co-segregation method. Nat Commun 2015;6(1). https://doi.org/10.1038/ncomms7519.

[16] Robinson JA. Growing vertical in the flatland. ACS Nano 2016;10(1):42–5.

[17] Wang S, Wang X, Warner JH. All chemical vapor deposition growth of mos₂:h-BN vertical van der Waals heterostructures. ACS Nano 2015;9(5):5246–54.

[18] Li Y, Xiong Y, Zhou Z, Tang B, Yang Z, Zhao J. The peeling behavior of nanowires and carbon nanotubes from a substrate using continuum modeling. J Appl Phys 2017;121(5):054303. https://doi.org/10.1063/1.4975054.

[19] Pan J, Ding D, Dong S, Liu Yu, Wei N, Zhao J. A theoretical analysis of peeling behavior between nanowires and substrates in the ambient condition with high relative humidity. Mech Mater 2017;114:243–53.

[20] Gigli L, Vanossi A, Tosatti E. Modeling nanoribbon peeling. Nanoscale 2019;11(37):17396–400.

[21] Chen H, Chen S. The peeling behaviour of a graphene sheet on a nano-scale corrugated surface. J Phys D-Appl Phys 2013;46(43):435305. https://doi.org/10.1088/0022-3727/46/43/435305.

[22] Zhang Y, Liu Q, Xu B. Liquid-assisted, etching-free, mechanical peeling of 2D materials. Extreme Mech Lett 2017;16:33–40.

[23] Tang D-M, Kvashnin DG, Najmaei S, Bando Y, Kimoto K, Koskinen P, et al. Nanomechanical cleavage of molybdenum disulphide atomic layers. Nat Commun 2014;5(1). https://doi.org/10.1038/ncomms4631.

[24] Lin K, Zhao Y-P. Mechanical peeling of van der Waals heterostructures: Theory and simulations. Extreme Mech Lett 2019;30:100501. https://doi.org/10.1016/j.eml.2019.100501.

[25] Stuart SJ, Tutein AB, Harrison JA. A reactive potential for hydrocarbons with intermolecular interactions. J Chem Phys 2000;112(14):6472–86.

[26] Brenner DW, Shenderova OA, Harrison JA, Stuart SJ, Ni B, Sinnott SB. A second-generation reactive empirical bond order (REBO) potential energy expression for hydrocarbons. J Phys-Condes Matter 2002;14(4):783–802.

[27] Chen Y, Zhang Y, Cai K, Jiang J, Zheng J-C, Zhao J, et al. Interfacial thermal conductance in graphene/black phosphorus heterogeneous structures. Carbon 2017;117:399–410.

[28] Liu Bo, Meng F, Reddy CD, Baimova JA, Srikanth N, Dmitriev SV, et al. Thermal transport in a graphene–mos₂ bilayer heterostructure: A molecular dynamics study. RSC Adv 2015;5(37):29193–200.

[29] Jiang J-W, Park HS. Molecular dynamics simulations of single-layer molybdenum disulphide (mos₂): Stillinger-Weber parametrization, mechanical properties, and thermal conductivity. J Appl Phys 2013;114(6):064307. https://doi.org/10.1063/1.4818414.

[30] Jones JE. On the determinations of molecular fields - I from the variation of the viscosity of a gas with temperature. Proc R soc Lond Ser A-Contain Pap Math Phys Character 1924;106(738):441–62.

[31] Jones JE. On the determination of molecular fields - II from the equation of state of a gas. Proc R soc Lond Ser A-Contain Pap Math Phys Character 1924;106(738):463–77.

[32] Jones JE. On the determination of molecular fields III - from crystal measurements and kinetic theory data. Proc R soc Lond Ser A-Contain Pap Math Phys Character 1924;106(740):709–18.

[33] Jiang J-W, Park HS. Mechanical properties of mos₂/graphene heterostructures. Appl Phys Lett 2014;105(3):033108. https://doi.org/10.1063/1.4891342.

[34] Ma Y, Dai Y, Guo M, Niu C, Huang B. Graphene adhesion on mos₂ monolayer: An ab initio study. Nanoscale 2011;3(9):3883–7.

[35] Zhao Y-P. Physical mechanics of surfaces and interfaces. Beijing: Science Press; 2012.

[36] Nosé S. A unified formulation of the constant temperature molecular dynamics methods. J Chem Phys 1984;81(1):511–9.

[37] Hoover WG. Canonical dynamics: Equilibrium phase-space distributions. Phys Rev A 1985;31(3):1695–7.

[38] Plimpton S. Fast parallel algorithms for short-range molecular dynamics. J Comput Phys 1995;117(1):1–19.

[39] Stukowski A. Visualization and analysis of atomistic simulation data with OVITO–the open visualization tool. Model Simul Mater Sci Eng 2010;18(1):015012. https://doi.org/10.1088/0965-0393/18/1/015012.

[40] Meyer JC, Geim AK, Katsnelson MI, Novoselov KS, Booth TJ, Roth S. The structure of suspended graphene sheets. Nature 2007;446(7131):60–3.

[41] Meyer JC, Geim AK, Katsnelson MI, Novoselov KS, Obergfell D, Roth S, et al. On the roughness of single- and bi-layer graphene membranes. Solid State Commun 2007;143(1–2):101–9.

[42] Xia M, Liang C, Cheng Z, Hu R, Liu S. The adhesion energy measured by a stress accumulation-peeling mechanism in the exfoliation of graphite. Phys Chem Chem Phys 2019;21(3):1217–23.

[43] Gao E, Lin S-Z, Qin Z, Buehler MJ, Feng X-Q, Xu Z. Mechanical exfoliation of two-dimensional materials. J Mech Phys Solids 2018;115:248–62.

[44] Zhao Y-P. Some new mesoscopic crossover length scales concerning the hamaker constant. Sci China-Technol Sci 2019;62(12):2310–2.

[45] Jiang LY, Huang Y, Jiang H, Ravichandran G, Gao H, Hwang KC, et al. A cohesive law for carbon nanotube/polymer interfaces based on the van der Waals force. J Mech Phys Solids 2006;54(11):2436–52.

[46] Zhao J, Lu L, Zhang Z, Guo W, Rabczuk T. Continuum modeling of the cohesive energy for the interfaces between films, spheres, coats and substrates. Comput Mater Sci 2015;96:432–8.

[47] Sauer RA. The peeling behavior of thin films with finite bending stiffness and the implications on gecko adhesion. J Adhes 2011;87(7–8):624–43.

[48] Sen D, Novoselov KS, Reis PM, Buehler MJ. Tearing graphene sheets from adhesive substrates produces tapered nanoribbons. Small 2010;6(10):1108–16.

[49] Tersoff J, Ruoff RS. Structural properties of a carbon-nanotube crystal. Phys Rev Lett 1994;73(5):676–9.

[50] Yakobson BI, Brabec CJ, Bernholc J. Nanomechanics of carbon tubes: Instabilities beyond linear response. Phys Rev Lett 1996;76(14):2511–4.

[51] Kudin KN, Scuseria GE, Yakobson BI. C_2F, BN, and C nanoshell elasticity from ab initio computations. Phys Rev B 2001;64(23):235406.

[52] Kendall K. Thin-film peeling-the elastic term. J Phys D-Appl Phys 1975;8(13):1449–52.

[53] Wang L-F, Ma T-B, Hu Y-Z, Zheng Q, Wang H, Luo J. Superlubricity of two-dimensional fluorographene/mos_2 heterostructure: A first-principles study. Nanotechnology 2014;25(38):385701. https://doi.org/10.1088/0957-4484/25/38/385701.

[54] Jiang J-W, Park HS. A Gaussian treatment for the friction issue of Lennard-Jones potential in layered materials: Application to friction between graphene, mos_2, and black phosphorus. J Appl Phys 2015;117(12):124304. https://doi.org/10.1063/1.4916538.

[55] Annett J, Cross GLW. Self-assembly of graphene ribbons by spontaneous self-tearing and peeling from a substrate. Nature 2016;535(7611):271–5.

[56] Korhonen T, Koskinen P. Peeling of multilayer graphene creates complex interlayer sliding patterns. Phys Rev B 2015;92(11):115427.

[57] Kendall K. The adhesion and surface energy of elastic solids. J Phys D-Appl Phys 1971;4(8):1186–95.

[58] Zhao Y-P. Nano and mesoscopic mechanics. Beijing: Science Press; 2014.

[59] Rivlin RS. The effective work of adhesion. In: Barenblatt GI, Joseph DD, editors. Collected papers of R.S. Rivlin. New York: Springer; 1997.

[60] Jin Y, Yuan FG. Simulation of elastic properties of single-walled carbon nanotubes. Compos Sci Technol 2003;63(11):1507–15.

[61] Huang Y, Wu J, Hwang KC. Thickness of graphene and single-wall carbon nanotubes. Phys Rev B 2006;74(24):245413.